

## LYMPHOID NEOPLASIA

# VAV1 mutations contribute to development of T-cell neoplasms in mice

Kota Fukumoto,<sup>1</sup> Mamiko Sakata-Yanagimoto,<sup>1-3</sup> Manabu Fujisawa,<sup>2</sup> Tatsuhiro Sakamoto,<sup>1-3</sup> Hiroaki Miyoshi,<sup>4</sup> Yasuhito Suehara,<sup>2,3</sup> Tran B. Nguyen,<sup>2</sup> Sakurako Suma,<sup>1</sup> Shintaro Yanagimoto,<sup>5</sup> Yuichi Shiraishi,<sup>6</sup> Kenichi Chiba,<sup>6</sup> Alyssa Bouska,<sup>7</sup> Keisuke Kataoka,<sup>8,9</sup> Seishi Ogawa,<sup>8</sup> Javeed Iqbal,<sup>7</sup> Koichi Ohshima,<sup>4</sup> and Shigeru Chiba<sup>1-3</sup>

<sup>1</sup>Department of Hematology, Comprehensive Human Biosciences, and <sup>2</sup>Department of Hematology, Faculty of Medicine, University of Tsukuba, Tsukuba, Japan; <sup>3</sup>Department of Hematology, University of Tsukuba Hospital, Tsukuba, Japan; <sup>4</sup>Department of Pathology, School of Medicine, Kurume University, Kurume, Japan; <sup>5</sup>Division for Health Service Promotion, University of Tokyo, Tokyo, Japan; <sup>6</sup>Division of Cellular Signaling, National Cancer Center Research Institute, Tokyo, Japan; <sup>7</sup>Department of Pathology and Microbiology, University of Nebraska Medical Center, Omaha, NE; <sup>8</sup>Department of Pathology and Tumor Biology, Graduate School of Medicine, Kyoto University, Kyoto, Japan; and <sup>9</sup>Division of Molecular Oncology, National Cancer Center Research Institute, Tokyo, Japan

## KEY POINTS

- Expression of VAV1 mutants on a p53-null background accelerated development of various types of TCNs.
- Myc pathway activation is marked in TCNs with VAV1 mutants, accompanying focal somatic copy-number alterations of the Myc locus.

**Activating mutations in the Vav guanine nucleotide exchange factor 1 (VAV1) gene are reported in various subtypes of mature T-cell neoplasms (TCNs). However, oncogenic activities associated with VAV1 mutations in TCNs remain unclear. To define them, we established transgenic mice expressing VAV1 mutants cloned from human TCNs. Although we observed no tumors in these mice for up to a year, tumors did develop in comparably aged mice on a p53-null background (p53<sup>-/-</sup> VAV1-Tg), and p53<sup>-/-</sup> VAV1-Tg mice died with shorter latencies than did p53-null (p53<sup>-/-</sup>) mice. Notably, various TCNs with tendency of maturation developed in p53<sup>-/-</sup> VAV1-Tg mice, whereas p53<sup>-/-</sup> mice exhibited only immature TCNs. Mature TCNs in p53<sup>-/-</sup> VAV1-Tg mice mimicked a subtype of human peripheral T-cell lymphoma (PTCL-GATA3) and exhibited features of type 2 T helper (Th2) cells. Phenotypes seen following transplantation of either p53<sup>-/-</sup> VAV1 or p53<sup>-/-</sup> tumor cells into nude mice were comparable, indicating cell-autonomous tumor-initiating capacity. Whole-transcriptome analysis showed enrichment of multiple Myc-related pathways in TCNs from p53<sup>-/-</sup> VAV1-Tg mice relative to p53<sup>-/-</sup> or wild-type T cells. Remarkably, amplification of the Myc locus was found recurrently in TCNs of p53<sup>-/-</sup> VAV1-Tg mice.**

**Finally, treatment of nude mice transplanted with p53<sup>-/-</sup> VAV1-Tg tumor cells with JQ1, a bromodomain inhibitor that targets the Myc pathway, prolonged survival of mice. We conclude that VAV1 mutations function in malignant transformation of T cells in vivo and that VAV1-mutant-expressing mice could provide an efficient tool for screening new therapeutic targets in TCNs harboring these mutations. (Blood. 2020;136(26):3018-3032)**

## Introduction

T-cell neoplasms (TCNs) are classified as mature TCNs (so-called peripheral T-cell lymphomas [PTCLs]) and immature TCNs (T-lymphoblastic lymphoma [T-LBL]) based on T-cell immunophenotypes. PTCLs are further subclassified as up to 30 categories based on pathological and clinical features.<sup>1</sup> Best standard-care protocols for TCNs have not been established due to lack of knowledge of molecular mechanisms. Recent genomic research has revealed the genetic landscape of PTCL and shown that PTCL driver mutations are highly enriched in factors functioning in survival and activation of normal T cells. Vav guanine nucleotide exchange factor (GEF) 1 (VAV1) is one of those genes genetically altered in various PTCL subtypes and encodes a factor that likely mediates physiological T-cell receptor (TCR) signaling. Frequencies of VAV1 alterations are 18% in adult T-cell lymphoma/leukemia (ATL),<sup>2</sup> 11% in anaplastic large-cell

lymphoma (ALCL), and 7% to 11% in PTCL not otherwise specified (PTCL-NOS).<sup>3-5</sup> In angioimmunoblastic T-cell lymphoma (AITL) and nodal PTCL with T-follicular helper (Tfh) phenotype (PTCL-Tfh), VAV1 mutation frequencies are as low as 5%.<sup>6,7</sup> However, the RHOAp.Gly17Val mutant, found in up to 70% of AITL, activates VAV1 by disrupting its autoinhibition, suggesting that VAV1 activation is more profoundly related to AITL pathogenesis than estimated from its mutation frequency.<sup>7</sup> On the other hand, VAV1 function in T-LBL is controversial, and VAV1 mutations are rarely found in human T-LBL samples.<sup>8</sup> Moreover, there is some evidence that VAV1 functions as a tumor suppressor in a mouse model of T-LBL.<sup>9</sup>

VAV1 is a member of VAV family proteins, consisting of VAV1, VAV2, and VAV3. VAV1 functions as a GEF, facilitating exchange of guanosine diphosphate (GDP) for guanosine triphosphate

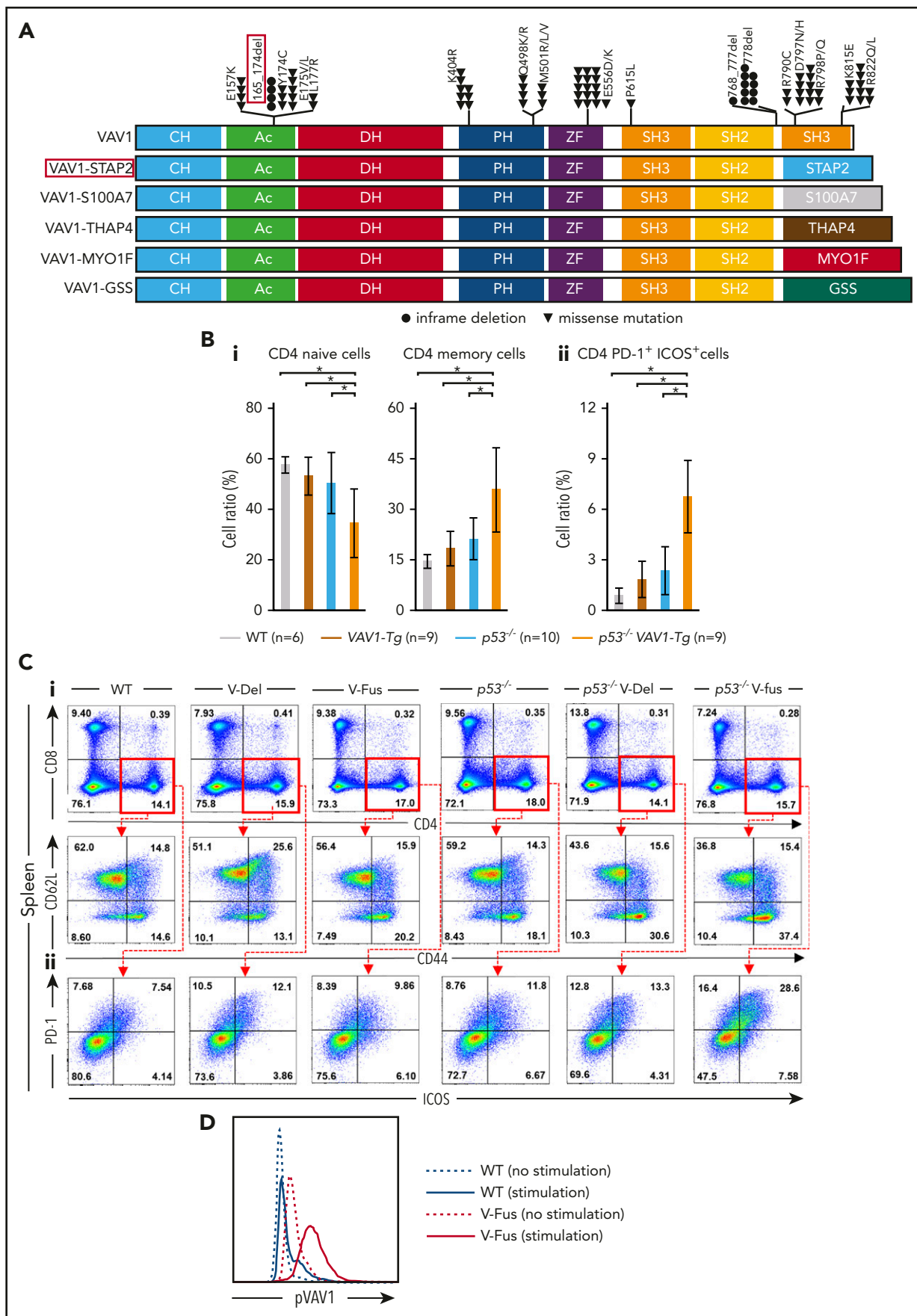


**Figure 1.**

(GTP).<sup>10</sup> TCR stimulation triggers VAV1 phosphorylation through Src family kinases such as LCK and FYN<sup>11-13</sup> at amino acid residues Tyr142, 160, and 174 in the acidic (Ac) domain, activating its GEF-dependent function to activate small GTPases such as Rac1 and its GEF-independent function as an adaptor enabling formation of a complex with Src homology 2 (SH2) domain-containing leukocyte protein of 76 kDa (SLP76) and phospholipase C,  $\gamma$  1 (PLCG1).<sup>14-16</sup> Vav1-deficient mice show partially impaired thymic T-cell development.<sup>17</sup> VAV1 deficiency in T cells also impairs the immune response after TCR stimulation.<sup>18,19</sup>

Mutations in VAV1 in PTCL occur in distinct patterns. Missense mutations accumulate at several hotspots in the Ac (Glu175), pleckstrin homology (PH; Lys404), zinc-finger (ZF; Glu556) and SH3 (Arg798 and Arg822) domains. Other mutations include focal in-frame deletions in the Ac domain ( $\Delta$ 165-174) or those in  $\Delta$ 778-786 in the C-terminal SH3 domain by alternative splicing, and fusion of VAV1 lacking the C-terminal SH3 domain with various partner genes (Figure 1A).<sup>2-7</sup> Alterations in either the Ac or SH3-SH2-SH3 domains impairs their interaction with the Dbl homology (DH) domain, disrupting autoinhibition.<sup>20,21</sup> Both alterations lead to hyperactivation of TCR signaling in vitro,<sup>7</sup> though how substitutions in the PH or ZF domains perturb downstream signaling remains unclear.

Here, we established transgenic mice expressing VAV1 mutants driven by the CD2 promoter to define their function in tumorigenesis in vivo.

## Methods

### Mice

Complementary DNAs (cDNAs) for a human VAV1 mutant (p.165\_174del) (V-Del) and a VAV1-STAP2 fusion gene mutant (V-Fus), identified in our PTCL cohort,<sup>7</sup> were cloned into a VA vector under control of the human CD2 promoter. Vectors were injected into fertilized eggs to generate V-Del and V-Fus transgenic mice on a C57BL/6 background. V-Del and V-Fus transgenic (VAV1-Tg) mice were crossed with *Trp53* knockout (*p53*<sup>-/-</sup>) mice to generate *p53*<sup>-/-</sup> V-Del or *p53*<sup>-/-</sup> V-Fus mice. Age-matched male nude mice served as recipients. All experiments were performed according to guidelines of the Laboratory Animal Resource Center in University of Tsukuba and approved by the Institutional Review Board (19-182).

### Whole-transcriptome analysis

Libraries for whole-transcriptome analysis (WTA) were made using a TruSeq RNA Sample Preparation Kit (Illumina) or SMARTer Stranded Total RNA-Seq Kit v2- Pico Input Mammalian<sup>22</sup> according to quantity of total RNA following the manufacturer's protocol. Sequencing was performed at Tsukuba i-Laboratory LLP (Ibaraki, Japan) using NextSeq 500 (Illumina) with a paired-end 36-base read option or at Macrogen Japan

(Kyoto, Japan) using HiSeqX (Illumina) with a paired-end 150-base read option.

### Whole-exome sequencing

Libraries for whole-exome sequencing (WES) were made using SureSelect XT Mouse All Exon Kits (Agilent Technologies) according to the manufacturer's instructions. Sequencing data were generated by standard 150-bp paired-end protocol. Sequence alignment and mutation calling were analyzed using the Genomon2 pipeline (<https://github.com/Genomon-Project>).

### Statistics

All statistical analyses were performed with EZR software (Saitama Medical Center, Jichi Medical University, Saitama, Japan).<sup>23</sup> Analysis of variance (ANOVA) was used with post hoc comparisons using Bonferroni method to determine differences between multiple groups. For comparison between 2 groups, the Student *t* test was performed. Survival was analyzed by the Kaplan-Meier method and differences between the curves were calculated by a 2-sided log-rank test. The Fisher exact test was used to compare frequencies of tumor subtypes.

### Other experimental methods

The detailed protocols for generation of mice, tumor cell transplantation, quantitative polymerase chain reaction (PCR), immunohistochemical staining, flow cytometry, TCR stimulation, WTA, WES, and in vivo treatment are described in supplemental Methods (available on the *Blood* Web site).

## Results

### Expression of VAV1 mutants in *p53*-null mice (*p53*<sup>-/-</sup> VAV1) promotes TCN development

To establish VAV1-mutant transgenic mice, we cloned 2 VAV1 cDNAs, V-Del and V-Fus, derived from human PTCL samples (Figure 1A)<sup>7</sup> into VA vectors in which transgenes were driven by the CD2 promoter (supplemental Figure 1A). Resultant vectors were injected into fertilized eggs to generate V-Del and V-Fus transgenic mice (supplemental Figure 1B). *TP53* alterations reportedly co-occur in some PTCL cases with VAV1 alterations (supplemental Figure 1C).<sup>24</sup> Thus, we crossed V-Del or V-Fus mice with conventional *p53*<sup>-/-</sup> mice to generate *p53*<sup>-/-</sup> V-Del or *p53*<sup>-/-</sup> V-Fus mice. VAV1 cDNA insertion and *Trp53* gene loss were confirmed by genomic PCR (supplemental Figure 1D).

We then evaluated blood counts and fractions of B, myeloid, and T cells in peripheral blood (PB) collected from mice of VAV1-Tg, *p53*<sup>-/-</sup>, or *p53*<sup>-/-</sup> VAV1-Tg genotypes and from wild-type (WT) controls at 8 weeks of age. The number of CD3<sup>+</sup> T cells significantly increased in blood of VAV1-Tg and *p53*<sup>-/-</sup> VAV1-Tg relative to WT mice (supplemental Figure 2A).

**Figure 1. Function of VAV1 mutations in physiological differentiation of splenic T cells.** (A) Schematic showing structures of VAV1-mutant proteins resulting from nonsynonymous mutations, in-frame deletions, and fusion with various partners identified in PTCL-NOS,<sup>3,5</sup> AITL,<sup>7</sup> ALCL,<sup>3</sup> and ATL.<sup>2</sup> (B) Cell fractions of splenocytes harvested from mice indicated genotypes at 12 weeks of age before tumor development. (i) Percentages of naive T cells defined by CD4<sup>+</sup>CD62L<sup>+</sup>CD44<sup>-</sup> and those of memory T cells defined by CD4<sup>+</sup>CD62L<sup>-</sup>CD44<sup>+</sup>. (ii) Percentage of CD4<sup>+</sup>PD-1<sup>+</sup>ICOS<sup>+</sup> cells. The number of mice analyzed is as follows: WT, n = 6; VAV1-Tg, n = 9; *p53*<sup>-/-</sup>, n = 10; *p53*<sup>-/-</sup> VAV1-Tg, n = 9. \**P* < .05. (C) Representative flow cytometric data indicating CD4 naive and memory T cells (i) and CD4<sup>+</sup>PD-1<sup>+</sup>ICOS<sup>+</sup> cells (ii) in indicated genotypes at 12 weeks of age. (D) Phosphorylated VAV1 (pVav1) protein expression examined by flow cytometry in naive T cells sorted from splenocytes of V-Fus or WT mice with or without TCR stimulation. Black line indicates WT; red line, V-Fus expression data. Dotted line indicates nonstimulated status; solid line, stimulated status.

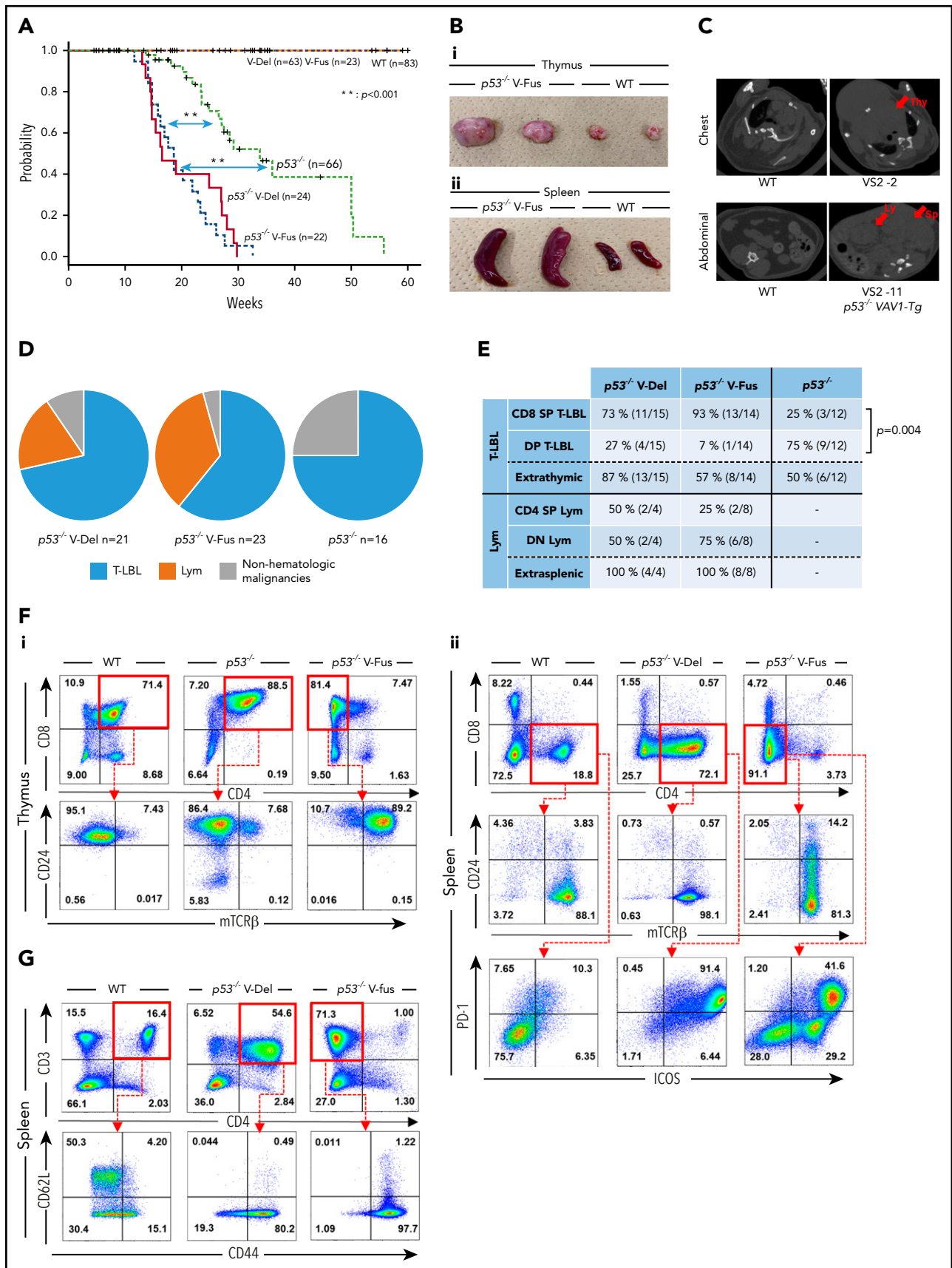


**Figure 2. Tumor development in  $p53$ -null mice expressing VAV1 mutants.** (A) OS of mice of indicated genotypes. (B) Macroscopic analysis of representative thymuses (i) at 12 weeks of age and spleens (ii) at 24 weeks of age from mice of indicated genotypes. (C) Representative data of chest (top) and abdominal (bottom) computed tomography scans, performed on  $p53^{-/-}$  V-Fus mice at 16 weeks (top) and 24 weeks (bottom) of age. WT mice served as controls. Arrows indicate a thymic tumor (Thy), swollen lymph node

At 12 weeks of age, we obtained single-cell suspensions of splenocytes and thymocytes from mice of each genotype for flow cytometry analysis. The frequencies of naive T cells, defined as CD4<sup>+</sup>CD62L<sup>+</sup>CD44<sup>-</sup>, significantly decreased, whereas the frequencies of memory T cells, defined as CD4<sup>+</sup>CD62L<sup>-</sup>CD44<sup>+</sup>, significantly increased in splenocytes from *p53*<sup>-/-</sup> VAV1-Tg relative to WT mice (Figure 1Bi,Ci). Notably, the number of CD4<sup>+</sup> cells expressing programmed cell death 1 (PD-1) and inducible T-cell costimulator (ICOS) significantly increased in splenocytes from *p53*<sup>-/-</sup> VAV1-Tg compared with WT mice (Figure 1Bii,Cii). In the thymus, the number of double negative 3 (DN3) cells, defined by CD44<sup>-</sup>CD25<sup>+</sup>, significantly increased in thymocytes from *p53*<sup>-/-</sup> VAV1-Tg relative to WT or *p53*<sup>-/-</sup> mice (supplemental Figure 2B-C). These data suggest overall that expression of VAV1 mutants on a *p53*-null background results in partially impaired thymocyte development at the DN3 stage and skewed expansion of splenic CD4<sup>+</sup> T cells.

We also examined phospho-VAV1 protein in naive T cells collected from either V-Fus or WT mice with or without TCR stimulation. Phospho-VAV1 expression levels were higher in cells from V-Fus mice than in those from WT mice with or without stimulation (Figure 1D).

Remarkably, *p53*<sup>-/-</sup> VAV1-Tg mice succumbed to tumors at shorter latencies than did *p53*<sup>-/-</sup> mice (Figure 2A). In contrast, VAV1-Tg mice on a WT background remained alive during the entire observation period, as did WT mice (>50 weeks; Figure 2A). To further enhance tumorigenicity, we irradiated either VAV1-Tg mice on a *p53*<sup>+/-</sup> background (*p53*<sup>+/-</sup> VAV1-Tg mice) or *p53*<sup>+/-</sup> mice at 4 Gy at ~8 weeks of age (supplemental Figure 3A). Irradiated *p53*<sup>+/-</sup> VAV1-Tg mice also showed shorter survival than irradiated *p53*<sup>+/-</sup> mice (supplemental Figure 3B).

Supplemental Table 1 summarizes distribution and immunophenotype of each tumor. Macroscopic observations and computed tomography scans revealed that tumor-bearing *p53*<sup>-/-</sup> VAV1-Tg mice displayed marked thymic enlargement or splenomegaly, sometimes accompanied by lymphadenopathy and extranodal tumors, whereas most tumor-bearing *p53*<sup>-/-</sup> mice showed only thymic enlargement (Figure 2B-C; supplemental Figure 3C; supplemental Table 1; and data not shown). We defined tumors as immature TCNs corresponding to human T-lymphoblastic lymphoma (T-LBL) and TCNs (lymphoma [Lym]) as mature (see "Flow cytometry" in supplemental Methods for details). Lym and T-LBL developed in *p53*<sup>-/-</sup> VAV1-Tg mice, whereas only T-LBL was seen in *p53*<sup>-/-</sup> mice (Figure 2D). The tumors also developed in irradiated *p53*<sup>+/-</sup> VAV1-Tg mice. *p53*<sup>+/-</sup> mice were either T-LBL or nonhematological malignancies as found in a *p53*-null background, whereas the WT *Trp53* allele was deleted in these tumors (supplemental Figure 3D).

The most frequently observed immunophenotypes in T-LBL were CD8<sup>+</sup> single-positive (SP) in *p53*<sup>-/-</sup> VAV1-Tg mice and CD4<sup>+</sup>CD8<sup>+</sup> double-positive (DP) in *p53*<sup>-/-</sup> mice. In addition, we observed TCNs with mature phenotypes in *p53*<sup>-/-</sup> VAV1-Tg mice in contrast to *p53*<sup>-/-</sup> mice, which developed only immature TCNs (*P* < .05) (Figure 2E). We also examined cell-surface expression of CD24 and membrane TCR (mTCR)  $\beta$ -chain (mTCR $\beta$ ), both of which reflect differentiation status,<sup>9</sup> by flow cytometry. T-LBL of *p53*<sup>-/-</sup> VAV1-Tg mice exhibited CD24<sup>+</sup>mTCR $\beta$ <sup>high+</sup>. In contrast, T-LBL from *p53*<sup>-/-</sup> mice displayed CD24<sup>+</sup>mTCR $\beta$ <sup>low+</sup> (Figure 2Fi). These data suggest that T-LBL samples from *p53*<sup>-/-</sup> VAV1-Tg mice are more mature than those from *p53*<sup>-/-</sup> mice.

Lym in *p53*<sup>-/-</sup> VAV1-Tg mice were mainly CD4<sup>-</sup>CD8<sup>-</sup> double negative (DN), although some were CD4<sup>+</sup> SP (Figure 2E). All Lym tumor cells exhibited a CD24<sup>-</sup>mTCR $\beta$ <sup>+</sup> mature T-cell phenotype and also expressed PD-1 and ICOS (Figure 2Fii) together with a CD44<sup>+</sup>CD62L<sup>-</sup> memory-like phenotype (Figure 2G).

Hematoxylin-eosin (HE)-stained sections showed that T-LBL thymus tissues were massively infiltrated by immature lymphocytes, and corticomedullary boundaries were disrupted (Figure 3Ai). Spleen from Lym samples exhibited enlarged follicles that were massively infiltrated by mature lymphocytes (Figure 3Aii). Lung and/or liver tissues were also infiltrated by tumor cells in some T-LBL and Lym samples (supplemental Figure 3E).

Analysis of CD3, CD4, and CD8 immunohistochemical staining in thymus and spleen from tumor-bearing *p53*<sup>-/-</sup> VAV1-Tg, *p53*<sup>-/-</sup>, and control WT mice confirmed T-LBL and Lym immunophenotypes determined by flow cytometry (Figure 3B). To evaluate the activation status of exogenous V-Fus mutant or endogenous VAV1 proteins in WT mice, we assessed phospho-VAV1 at Tyr174 by immunohistochemical staining (note that V-Del mutant protein lacks Tyr174 and cannot be similarly evaluated). We detected phospho-VAV1 only in spleen tissues from Lym samples from *p53*<sup>-/-</sup> V-Fus mice (Figure 3Bi-ii).

We then evaluated serum cytokine concentrations in tumor-bearing *p53*<sup>-/-</sup> VAV1-Tg, *p53*<sup>-/-</sup>, and control WT mice at 16 weeks of age. Interleukin-4 (IL-4), IL-6, and IL-10 levels significantly increased in *p53*<sup>-/-</sup> VAV1-Tg mice harboring Lym relative to WT or *p53*<sup>-/-</sup> mice with T-LBL or *p53*<sup>-/-</sup> VAV1-Tg mice with T-LBL (Figure 3C). These data suggest overall that *p53*<sup>-/-</sup> VAV1-Tg mice harboring Lym exhibit skewed commitment toward a type 2 T helper (Th2) phenotype.

In summary, we observed TCNs with mature phenotypes in *p53*<sup>-/-</sup> VAV1-Tg mice in contrast to *p53*-null mice, which developed only immature TCNs.

**Figure 2 (continued)** (Ly) and enlarged spleen (Sp), respectively. (D) Subtypes of tumors found in mice of indicated genotypes (*p53*<sup>-/-</sup> V-Del, *n* = 21; *p53*<sup>-/-</sup> V-Fus, *n* = 23; *p53*<sup>-/-</sup>, *n* = 16). Immature T-cell neoplasms (T-lymphoblastic lymphomas [T-LBL]) are shown in blue; mature T-cell neoplasms (lymphoma [Lym]) in orange; and nonhematological malignancies in gray. (E) Cell-surface immunophenotypes of CD4 and CD8 cells from T-LBL or Lym from mice of indicated genotypes. (F) Representative flow cytometric data of CD4 and CD8, and CD24 and mTCR $\beta$  as indicators of cell-maturation status, and PD-1 and ICOS, indicating cell-activation status for thymocytes from *p53*<sup>-/-</sup> V-Fus and *p53*<sup>-/-</sup> mice harboring T-LBL plus WT mice (i) and splenocytes from *p53*<sup>-/-</sup> V-Del and *p53*<sup>-/-</sup> V-Fus mice harboring Lym plus WT mice (ii). (G) Representative flow cytometric data to show naive-like (CD4<sup>+</sup>CD62L<sup>+</sup>CD44<sup>-</sup>) and memory-like (CD4<sup>+</sup>CD62L<sup>-</sup>CD44<sup>+</sup>) phenotypes for splenocytes from *p53*<sup>-/-</sup> V-Del and *p53*<sup>-/-</sup> V-Fus mice harboring Lym plus WT mice. DN, double negative; DP, double positive; SP, single positive.

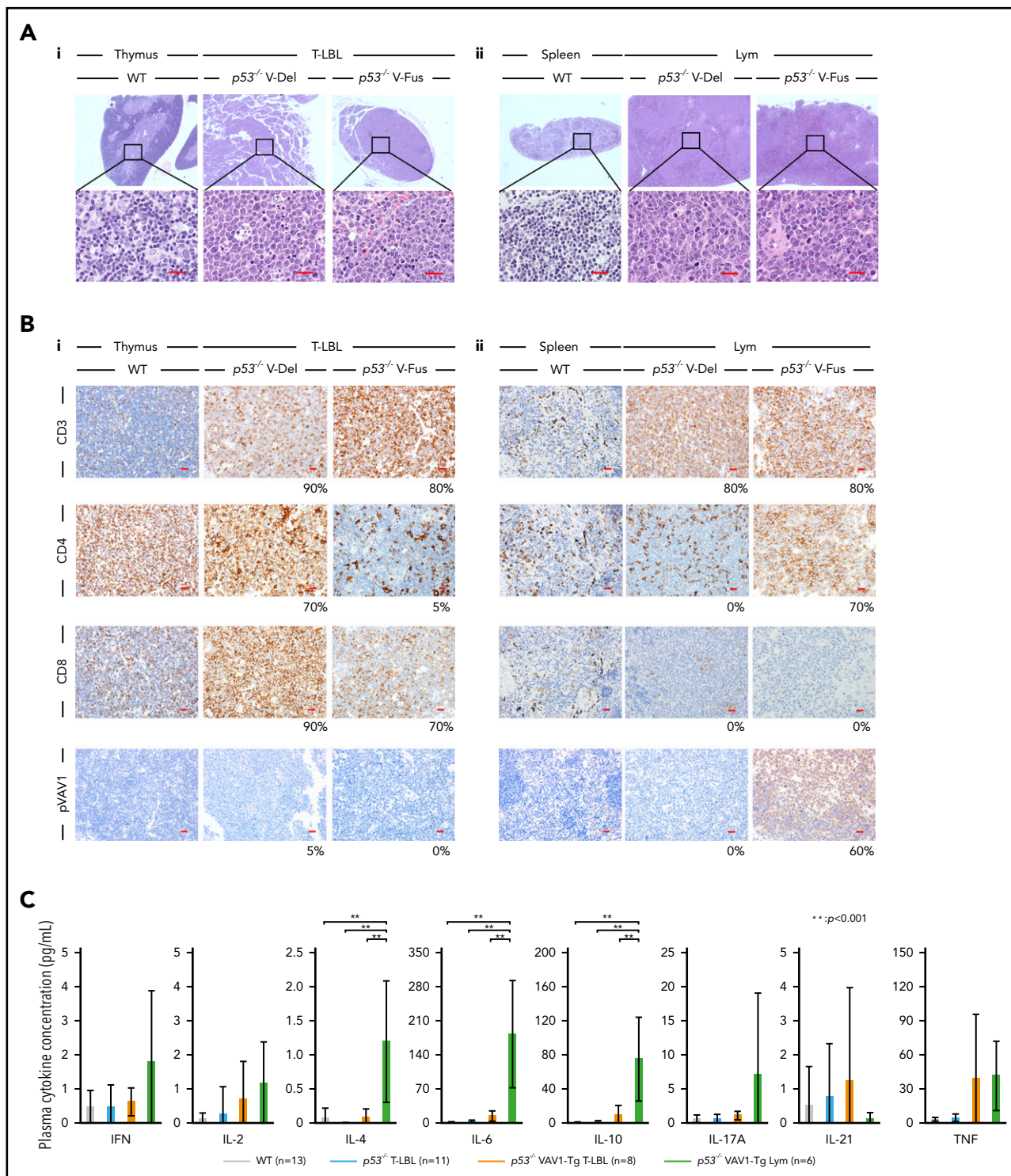


**Figure 3. Characterization of tumors found in VAV1-mutant  $p53$ -null mice.** (A) Sections stained by hematoxylin-eosin (HE) for tumors collected from mice of indicated genotypes. (i) Thymuses from indicated mutant mice harboring T-LBL plus control WT mice. (ii) Splenes from indicated mutant mice harboring Lym plus WT mice. Original magnification:  $\times 4$ ; insets,  $\times 100$ . Scale bars,  $20\ \mu\text{m}$ . (B) Immunohistochemical analysis of CD3, CD4, CD8a, and phosphorylated-VAV1 (pVAV1). (i) Thymuses from indicated mutant mice harboring T-LBL or WT mice. (ii) Splenes from indicated mutant mice harboring Lym or WT mice. Original magnification  $\times 40$ . Scale bars,  $20\ \mu\text{m}$ . The percentages at the bottom right corner of figures for both T-LBL and Lym samples indicate the positivity in the tumor cells. (C) Serum cytokines measured in blood of tumor-bearing mice of indicated genotypes measured at 16 to 24 weeks as control WT mice. The number of mice analyzed is as follows: WT,  $n = 13$ ;  $p53^{-/-}$  mice bearing T-LBL,  $n = 11$ ;  $p53^{-/-}$  VAV1-Tg mice bearing T-LBL,  $n = 8$ ;  $p53^{-/-}$  VAV1-Tg mice bearing Lym,  $n = 6$ . \*\* $P < .001$ .

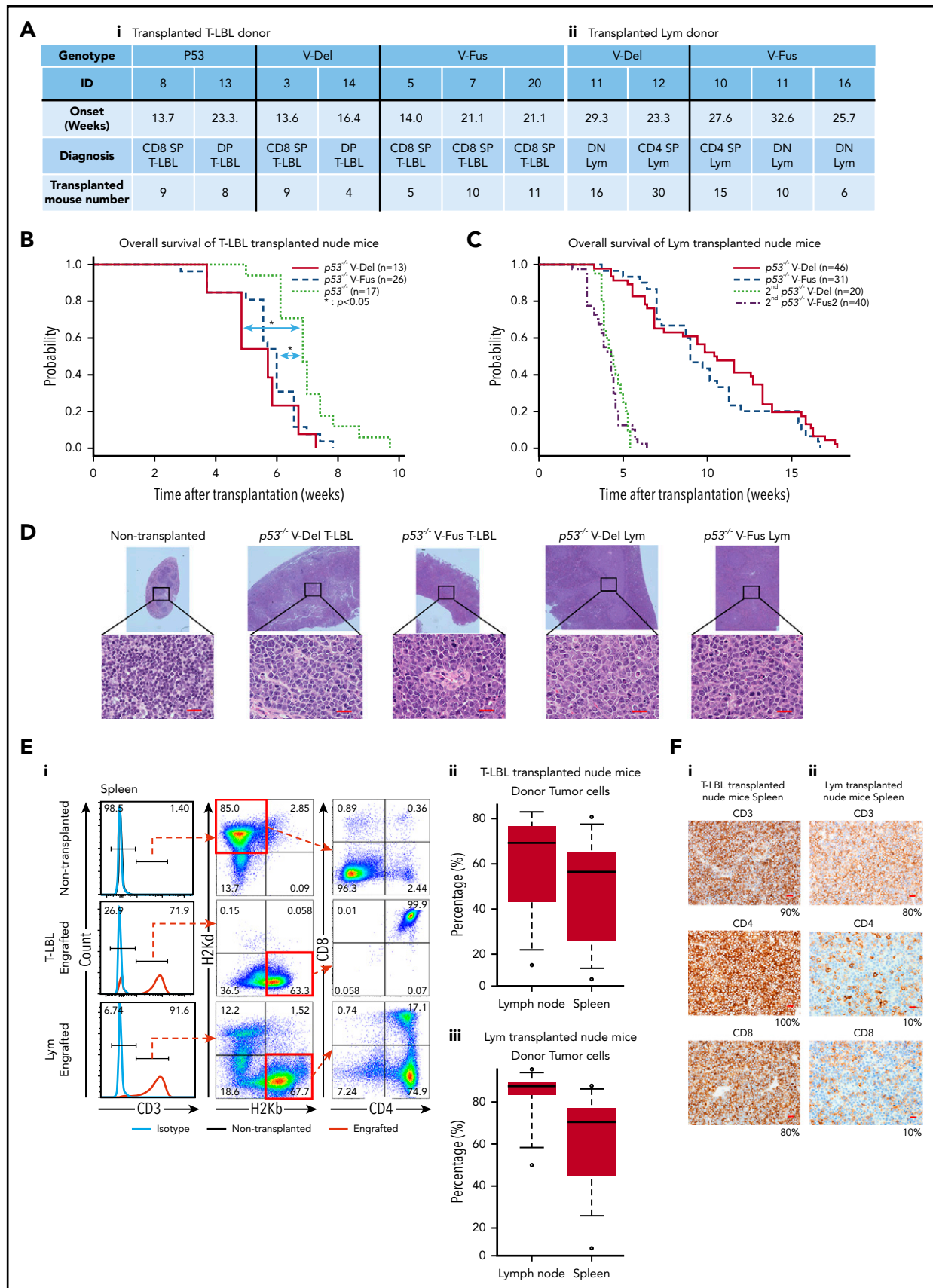


**Figure 4. Tumor-initiating capacity of tumor cells found in  $p53^{-/-}$  VAV1-Tg and  $p53^{-/-}$  mice.** (A) Summary of donor mice, showing genotypes and various experimental parameters. The summary of transplanted T-LBL donor mice (i) and Lym donor mice (ii). (B) OS of nude mice transplanted intraperitoneally with T-LBL of indicated genotypes ( $p53^{-/-}$  V-Del,  $n = 13$ ;  $p53^{-/-}$  V-Fus,  $n = 26$ ; and  $p53^{-/-}$ ,  $n = 17$ ). (C) OS of nude mice that were initially and then secondarily transplanted with Lym from  $p53^{-/-}$  VAV1-Tg mice

## **$p53^{-/-}$ VAV1-mutant and $p53^{-/-}$ tumor cells show cell-autonomous transforming activity**

To assess cell-autonomous activity of tumor cells seen in  $p53^{-/-}$  VAV1-Tg and  $p53^{-/-}$  mice, we prepared single-cell suspensions from thymic tumors of  $p53^{-/-}$  VAV1-Tg and  $p53^{-/-}$  mice harboring T-LBL and from enlarged spleens of  $p53^{-/-}$  VAV1-Tg mice harboring Lym (Figure 4A). These donor cells were injected intraperitoneally into immunodeficient BALB-c/ $\nu$  mice (nude mice) after 2 Gy irradiation. The recipient mice transplanted with T-LBL from  $p53^{-/-}$  VAV1-Tg mice gradually succumbed to tumors at shorter latencies than those with  $p53^{-/-}$  T-LBL (Figure 4B). In addition, Lym samples from  $p53^{-/-}$  VAV1-Tg mice were also transplantable into nude mice, though latencies for tumor development were longer than those with T-LBL, whereas secondarily transplanted mice succumbed to tumors with shorter latencies (Figure 4C). Macroscopically, the recipient mice transplanted with either T-LBL or Lym displayed marked splenomegaly, lymphadenopathy, liver enlargement, and ascites (data not shown). HE-stained sections of spleen from the engrafted recipient mice showed that follicles were enlarged and massively infiltrated by tumor cells (Figure 4D). Significant proportions of cells in spleens and lymph nodes of the recipient mice transplanted with either T-LBL or Lym were donor-derived, as indicated by H-2K<sup>b</sup> positivity (Figure 4E). Flow cytometry and immunohistochemical staining showed that tumor cell immunophenotypes in recipients mimicked those of donor cells (Figure 4F and data not shown). Genomic PCR performed in tumor tissues from the recipient mice confirmed that donor cells exhibited integration of human VAV1 and partial deletion of *Trp53* gene, as recipient cells harboring WT *Trp53* were found in tumor tissues (supplemental Figure 4).

We conclude that tumor cells from both T-LBL and Lym samples have tumor-initiating activity.

## **Gene-expression profiles of tumors harboring VAV1 mutants**

To define molecular mechanisms underlying tumorigenesis, we next performed WTA using RNA extracted from whole thymocytes from the following groups: (1) T-LBL from  $p53^{-/-}$  VAV1-Tg mice (>90% were tumor cells [ $n = 4$ :  $p53^{-/-}$  V-Del,  $n = 2$ ;  $p53^{-/-}$  V-Fus,  $n = 2$ ]), (2) T-LBL from  $p53^{-/-}$  mice (>90% were tumor cells,  $n = 2$ ), (3) CD4/CD8-DP thymocytes from WT mice ( $n = 3$ ), (4) a tumor cell fraction (CD4/CD8 DN or CD4 SP) of splenocytes from Lym from  $p53^{-/-}$  VAV1-Tg mice ( $n = 5$ :  $p53^{-/-}$  V-Del,  $n = 3$ ;  $p53^{-/-}$  V-Fus mice,  $n = 2$ ), and (5) CD4-SP or CD8-SP splenocytes of WT mice ( $n = 6$ : CD4 SP,  $n = 3$ ; CD8 SP,  $n = 3$ ).

Principal component analysis and unsupervised clustering revealed a distinct gene-expression pattern in each group of tumor cells (Figure 5A; supplemental Figure 5A). We then determined genes highly expressed in tumors with VAV1 mutations

by comparing a list of genes more highly expressed in T-LBL from  $p53^{-/-}$  VAV1-Tg compared with  $p53^{-/-}$  mice as well as those more highly expressed in Lym from  $p53^{-/-}$  VAV1-Tg compared with splenocytes of WT mice. We identified 176 genes showing a twofold change and 36 genes showing a threefold change common to both lists (Figure 5B; supplemental Figure 5B; supplemental Table 2). Remarkably, *Myc* was one of the genes most highly expressed in VAV1-mutant tumors (Figure 5C). We also examined the *Myc* expression levels by quantitative PCR analysis for T-LBL of  $p53^{-/-}$  VAV1-Tg mice ( $n = 8$ ) and that of  $p53^{-/-}$  mice ( $n = 6$ ). We confirmed that *Myc* expression levels were significantly higher in T-LBL of  $p53^{-/-}$  VAV1-Tg T-LBL than that of  $p53^{-/-}$  T-LBL (supplemental Figure 5C). Metascape analysis<sup>25</sup> for genes highly expressed in VAV1-mutant tumors indicated enrichment of cell-cycle-related pathways (supplemental Figure 5D; supplemental Table 3).

We then performed gene-set enrichment analysis (GSEA)<sup>26,27</sup> for WTA data. Analysis of the Hallmark gene matrix analysis in the Molecular Signature Database (MSigDB) indicated significant enrichment of multiple oncogenic pathways, including the G2M checkpoint, E2F targets, and phosphatidylinositol 3-kinase-AKT-mammalian target of rapamycin signaling in T-LBL from  $p53^{-/-}$  VAV1-Tg relative to  $p53^{-/-}$  mice (supplemental Figure 5E; supplemental Table 4). Notably, most gene sets significantly enriched in T-LBL from  $p53^{-/-}$  VAV1-Tg mice were also significantly enriched in Lym tumors from  $p53^{-/-}$  VAV1-Tg mice (supplemental Figure 5E; supplemental Table 4). Analysis of curated gene sets in the MSigDB indicated enrichment of multiple MYC-related gene sets in both T-LBL and Lym from  $p53^{-/-}$  VAV1-Tg mice (Figure 5D-E; supplemental Table 5).

We further evaluated Lym features seen in  $p53^{-/-}$  VAV1-Tg mice to determine what type of human TCNs these tumors reflected. Although Lym tumor cells expressed PD-1 and ICOS, both used for classification of Tfh phenotypes in the World Health Organization (WHO) classification for human TCNs,<sup>1</sup> gene-expression profiles (GEPs) of Lym samples did not show enrichment of a Tfh signature; in contrast, we observed clear enrichment of a Tfh signature in tumors from AITL model mice expressing the G17V *RHOA* mutation on a *Tet2*-null background<sup>28</sup> (Figure 5F). Remarkably, we observed enrichment of a Th2 signature in Lym samples from  $p53^{-/-}$  VAV1-Tg mice relative to WT CD4 splenocytes (supplemental Figure 5F). These data suggest that Lym from  $p53^{-/-}$  VAV1-Tg mice mimic a subtype of peripheral T-cell lymphoma (PTCL-GATA3) among human TCNs. Flow cytometry analysis also revealed expression of Ccr4, a marker of PTCL-GATA3, in these Lym tumor cells (Figure 5Gi). Gata3 protein expression was also confirmed by both flow cytometry analysis and immunohistochemical staining in these cells (Figure 5Gii,H).

Notably, GSEA showed that gene sets, including genes more highly expressed in human PTCL-GATA3 specimens with both

**Figure 4 (continued)** ( $p53^{-/-}$  V-Del,  $n = 46$ ;  $p53^{-/-}$  V-Fus,  $n = 31$ ; 2nd  $p53^{-/-}$  V-Del,  $n = 20$ ; 2nd  $p53^{-/-}$  V-Fus,  $n = 40$ ). (D) HE-stained sections from nude mice transplanted with T-LBL or Lym of indicated genotypes. Original magnification:  $\times 4$ ; insets,  $\times 100$ . Scale bars, 20  $\mu\text{m}$ . (E) Characterization of donor-derived cells in spleens and lymph nodes. (i) Representative flow cytometric analysis for CD3, CD4, and CD8 to determine immunophenotypes of tumor cells, and H2Kd and H2Kb, MHC class I molecules to determine recipient-derived ( $\nu/\nu$ ) and donor-derived (C57BL/6) cells, respectively. (ii) Percentages of donor cells in lymph nodes and spleens of nude mice transplanted with T-LBL. (iii) Percentages of donor cells in lymph nodes and spleens of nude mice transplanted with Lym. (F) Immunohistochemical analysis for CD3, CD4, and CD8 in spleens of nude mice transplanted with T-LBL (i) and Lym (ii) from  $p53^{-/-}$  VAV1-Tg mice. Original magnification  $\times 40$ . Scale bars, 20  $\mu\text{m}$ . The percentage at the bottom right corner is positivity in the tumor cells.



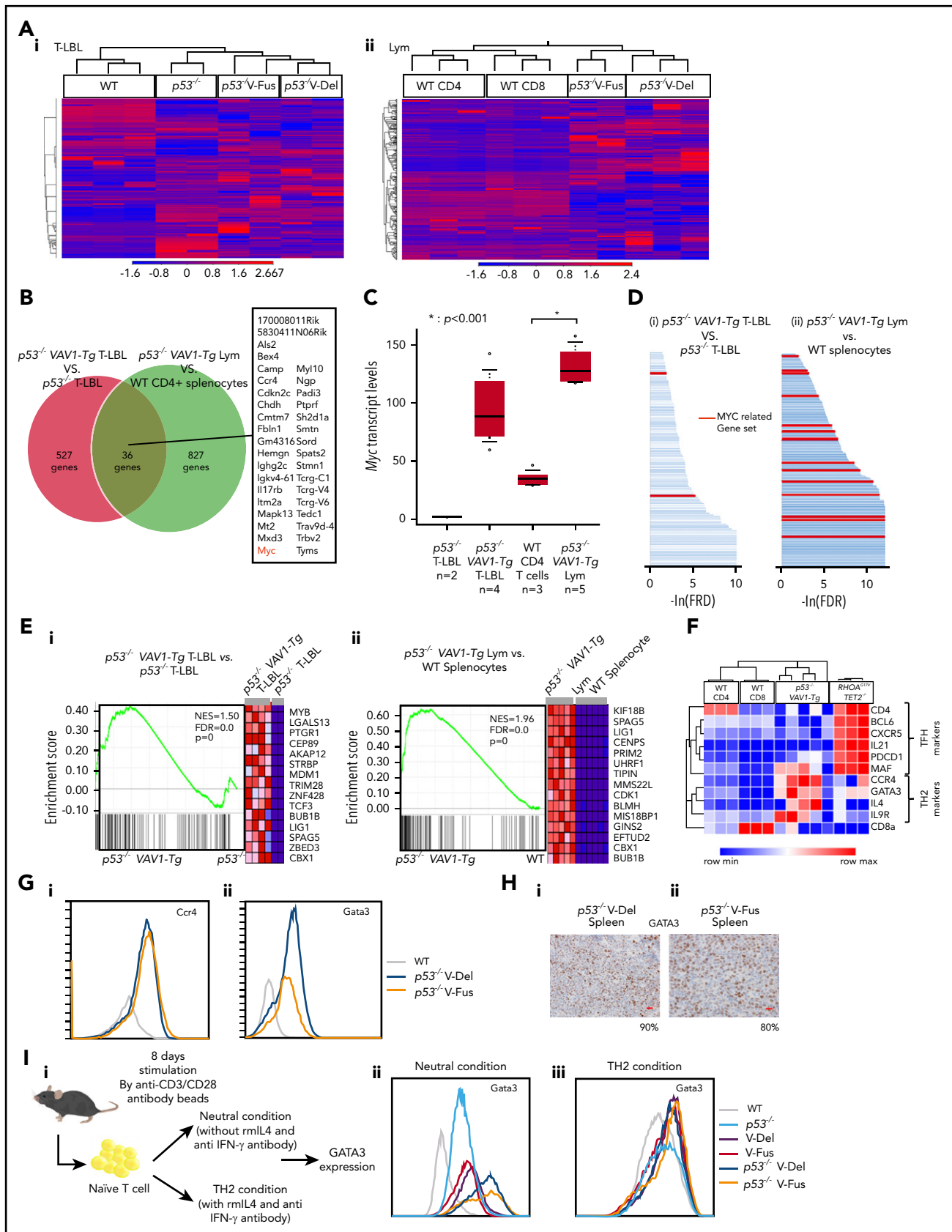


**Figure 5. WTAs for tumors found in  $p53^{-/-}$  VAV1-Tg or  $p53^{-/-}$  mice.** (A) Unsupervised hierarchical clustering analyses for T-LBL from mice of indicated genotypes and whole thymocytes from WT mice (i), and tumor cells sorted from Lym from mice of indicated genotypes and CD4<sup>+</sup> or CD8<sup>+</sup> splenocytes from WT mice (ii). (B) Venn diagram of genes expressed at threefold higher levels in T-LBL from  $p53^{-/-}$  VAV1-Tg mice relative to  $p53^{-/-}$  mice, or levels seen in Lym from  $p53^{-/-}$  VAV1-Tg mice relative to CD4<sup>+</sup> splenocytes. Thirty-six genes highly expressed in both of T-LBL and Lym of  $p53^{-/-}$  VAV1-Tg mice compared with controls are listed. (C) *Myc* expression levels in T-LBL from  $p53^{-/-}$  mice of (n = 2), and

VAV1 and TP53 alterations than those in PTCL-GATA3 specimens with TP53 alterations but without VAV1, tended to be enriched in tumors from  $p53^{-/-}$  VAV1-Tg mice comparing to those from  $p53^{-/-}$  mice. Conversely, gene sets including genes more highly expressed in tumors from  $p53^{-/-}$  VAV1-Tg mice than from  $p53^{-/-}$  mice tended to be enriched in human PTCL-GATA3 specimens with VAV1 and TP53 alterations (supplemental Figure 5G).

### GEPs of T cells from non-tumor-bearing mice

Next, we examined the GEPs of T cells from non-tumor-bearing mice with each genotype. WTA was performed using RNA from CD4<sup>+</sup> naive T cells (CD4 T<sub>N</sub>) and memory T cells (CD4 T<sub>mem</sub>) sorted from whole spleen of the following non-tumor-bearing mice at 12 weeks of age: (1)  $p53^{-/-}$  VAV1-Tg mice, (2)  $p53^{-/-}$  mice, and (3) WT mice. We found that *Myc* expression was significantly higher in CD4 T<sub>N</sub> from  $p53^{-/-}$  V-Fus mice than in CD4 T<sub>N</sub> from WT mice (supplemental Figure 6Ai) and in CD4 T<sub>mem</sub> from  $p53^{-/-}$  V-Fus mice than in CD4 T<sub>mem</sub> from  $p53^{-/-}$  mice (supplemental Figure 6Bi). In addition, *Gata3* expression was significantly higher in CD4 T<sub>mem</sub> from  $p53^{-/-}$  V-Fus mice than in CD4 T<sub>mem</sub> from  $p53^{-/-}$  mice (supplemental Figure 6Bii). Notably, we identified by GSEA that G2M checkpoint and E2F targets were commonly enriched in CD4 T<sub>mem</sub> from  $p53^{-/-}$  V-Fus mice compared with CD4 T<sub>mem</sub> from WT mice and in Lym from  $p53^{-/-}$  VAV1-Tg mice compared with CD4<sup>+</sup> splenocytes from WT mice (supplemental Figure 6D-E; supplemental Table 4). Notably, inflammatory-related pathways were also enriched in both CD4 T<sub>N</sub> and CD4 T<sub>mem</sub> from  $p53^{-/-}$  V-Fus mice comparing to those from  $p53^{-/-}$  or WT mice, although enrichment of these pathways was not observed in *Vav1*-mutated tumors (supplemental Figure 6C-E; supplemental Table 4).

Therefore, enrichment of cell-cycle-related pathways such as G2M checkpoint and E2F targets and slightly higher levels of *Myc* and *Gata3* were observed in CD4 T cells of  $p53^{-/-}$  VAV1-Tg mice even at non-tumor-bearing status, whereas enrichment of multiple oncogenic pathways, especially those related to *Myc*, was only observed in tumors of these mice.

To examine the skewed differentiation of naive T cells collected from mice with each genotype, we stimulated naive T cells by anti-CD3/CD28 microbeads without any other cytokines or antibodies ("neutral condition") or in the presence of IL-4 and anti-IFN- $\gamma$  antibody, which have been widely used for induction of Th2 cells ("Th2 condition"); *Gata3* expression levels were then examined (Figure 5I). In the neutral condition, the *Gata3* expression levels were the highest in cells from  $p53^{-/-}$  VAV1-Tg mice than in those with the other genotypes, whereas the levels were higher in cells from VAV1-Tg mice than those from WT or  $p53^{-/-}$  mice (Figure 5Iii). VAV1 mutant did not affect the *Gata3* expression levels in the Th2 condition (Figure 5Iiii). These data

suggest that mutant VAV1 induces Th2 skewing, which is further augmented by deletion of the *Trp53* gene.

### Clonal architecture of tumors harboring VAV1 mutants

To assess clonal architecture of T-LBL and Lym tumor cells, we performed WES analysis of paired tumors plus tails (as normal controls) collected from 17 mice (7  $p53^{-/-}$  VAV1-Tg<sup>LBL</sup>, 7  $p53^{-/-}$  VAV1-Tg<sup>Lym</sup>, and 3  $p53^{-/-}$  LBL). In total, we detected 132 somatic mutations, including 111 single-nucleotide variants (SNVs), 18 insertions and deletions (indels), and 3 nonsense mutations. The percentage of targeted bases covered by 2 $\times$ , 10 $\times$ , 20 $\times$ , 30 $\times$ , 40 $\times$ , 50 $\times$ , and 100 $\times$  sequencing average reads is shown in Figure 6A. Average read depth varied from 77.1 to 133.7 (supplemental Figure 7A). WES analysis identified 2 recurrent mutations: *Notch1* mutations in tumors from both  $p53^{-/-}$  VAV1-Tg mice and  $p53^{-/-}$  mice, and *Ddx3x* mutations in  $p53^{-/-}$  VAV1-Tg mice only.  $p53^{-/-}$  VAV1-Tg mice also exhibited *Jak1* and *Tet2* mutations, which are seen in human ATL/PTCL-NOS (Figure 6B; supplemental Table 6).

We then analyzed somatic copy-number alterations (SCNAs) using the WES data. In total, 5 focal SCNAs were identified: 2 amplifications (14qE1 and 15qD1) and 3 deletions (6qB1, 14aC2, and 16qA1) (Figure 6C). Notably, focal SCNAs of 15qD1, including the *Myc* locus, were recurrently observed in tumors of 4  $p53^{-/-}$  VAV1-Tg mice (1 of 7 T-LBL, and 3 of 7 Lym), but were not detected in T-LBL from  $p53^{-/-}$  mice (supplemental Table 7). Two tumors from  $p53^{-/-}$  VAV1-Tg mice showed high-level (more than eightfold) amplification of 15qD1, including the *Myc* locus (Figure 6D).

Actually, *Myc* protein was highly expressed in CD3<sup>+</sup> T-LBL and Lym tumor cells from  $p53^{-/-}$  VAV1-Tg mice but was only minimally expressed in equivalent cells from  $p53^{-/-}$  mice (Figure 6E; supplemental Figure 7B). In contrast, at 12 weeks of age, *Myc* protein was detected only in a minimal number of thymus and spleen cells in V-Fus,  $p53^{-/-}$ , and  $p53^{-/-}$  V-Fus mice (supplemental Figure 7C), although as shown in supplemental Figures 6Ai,Bi, *Myc* messenger RNA upregulation was observed in splenic CD4 T<sub>N</sub> and T<sub>mem</sub> cells from  $p53^{-/-}$  V-Fus mice at this time period (supplemental Figure 6Ai,Bi).

Figure 6F summarizes recurrent gene mutations and focal SCNAs. Finally, application of the MiXCR algorithm using WES data identified clonal rearrangements of at least 1 of the *TCR* genes in all tumors (Figure 6G; supplemental Figure 7D), supporting clonal expansion of T-lineage cells in all the tumors. Additionally, all tumors except for 1 had rearrangements of *TCR*  $\beta$ -chain genes. Lym tumors always had rearrangements of *TCR*  $\alpha$ -chain genes, whereas some T-LBL also had rearrangements.

**Figure 5 (continued)**  $p53^{-/-}$  VAV1-Tg mice (n = 4), and in CD4<sup>+</sup> splenocytes from WT mice (n = 3), and Lym from  $p53^{-/-}$  VAV1-Tg mice (n = 5). (D) Significantly enriched gene sets identified by GSEA using curated gene sets in the Molecular Signatures Database.<sup>26,27</sup> T-LBL from  $p53^{-/-}$  VAV1-Tg mice vs T-LBL from  $p53^{-/-}$  mice (i), and tumor cells sorted from Lym from  $p53^{-/-}$  VAV1-Tg mice vs CD4<sup>+</sup> and CD8<sup>+</sup> splenocytes from WT mice (ii). Red lines indicate MYC-related gene sets. (E) Representative results of enrichment plots of *Myc*-related gene sets. T-LBL from  $p53^{-/-}$  VAV1-Tg mice vs T-LBL from  $p53^{-/-}$  mice (i), and tumor cells sorted from Lym from  $p53^{-/-}$  VAV1-Tg mice vs CD4<sup>+</sup> or CD8<sup>+</sup> splenocytes from WT mice (ii). (F) GEPs of WT CD4<sup>+</sup> or CD8<sup>+</sup> splenocytes, tumor cells sorted from Lym from  $p53^{-/-}$  VAV1-Tg mice, and cells from ATL-like tumors in *RHOA*<sup>G17V</sup> *Tet2*<sup>-/-</sup> mice.<sup>28</sup> (G) Cell-surface expression of Ccr4 and *Gata3* analyzed by flow cytometry. (H) Immunohistochemical analysis for *Gata3* in spleens of Lym from  $p53^{-/-}$  VAV1-Tg mice. Original magnification  $\times 40$ . Scale bars, 20  $\mu$ m. The percentages at the bottom right corner indicate positivity in the tumor cells. (I) Schema showing a protocol for skewed differentiation of naive T cells sorted from splenocytes with each genotype. Cells were cultured in neutral condition without any cytokines or antibodies and Th2 condition with recombinant mouse IL-4 and anti-IFN- $\gamma$  antibody, respectively. *Gata3* expression levels were examined by flow cytometry 8 days after TCR stimulation.

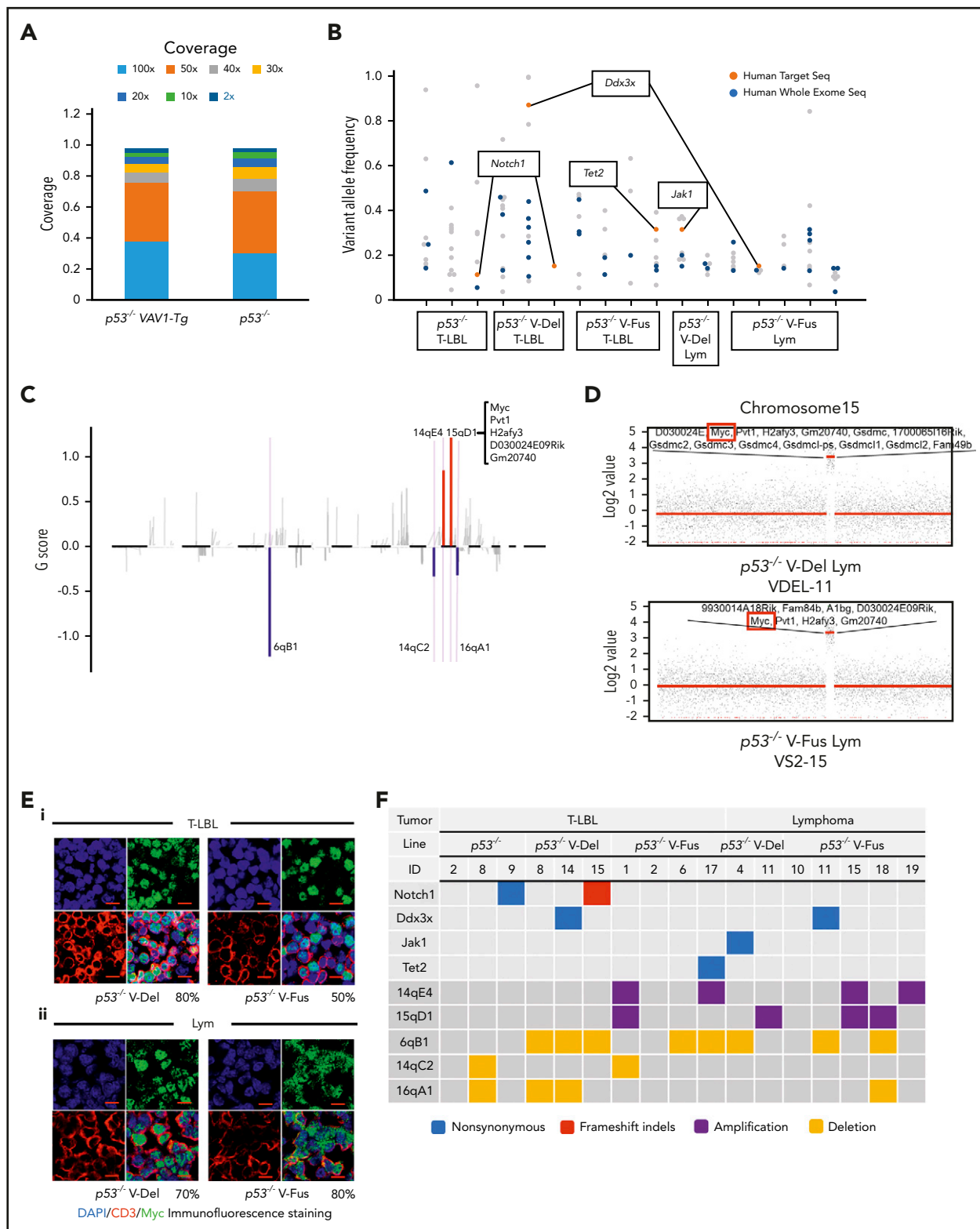


**Figure 6. WES analysis of tumor and tail samples.** (A) Percentages of targeted bases covered by at least 2×, 10×, 20×, 30×, 40×, 50×, and 100× sequencing reads (top). (B) Variant allele frequencies of somatic mutations in each tumor (T-LBL from p53<sup>-/-</sup> mice, n = 3; T-LBL from p53<sup>-/-</sup> V-Del, n = 3; T-LBL from p53<sup>-/-</sup> V-Fus, n = 4; Lym from p53<sup>-/-</sup> V-Del, n = 2; and Lym from p53<sup>-/-</sup> V-Fus, n = 5). Mutations identified in human targeted capture sequencing data<sup>24</sup> are shown in orange, and those identified in human WES data<sup>2</sup> in blue. (C) Focal SCNAs identified through the GISTIC 2.0 algorithm using WES data. Amplified regions are shown in red; deleted regions are shown in blue. Chromosome 15qD1 includes the *Myc* locus. (D) High-level amplification of the *Myc* locus identified in Lym from 2 p53<sup>-/-</sup> VAV1-Tg mice. (E) Immunofluorescent staining for indicated markers in thymus from p53<sup>-/-</sup> V-Del and p53<sup>-/-</sup> V-Fus mice harboring T-LBL (i), and in spleens of p53<sup>-/-</sup> V-Del and p53<sup>-/-</sup> V-Fus mice harboring Lym (ii). Original magnification ×400. Scale bars, 10 μm. The percentage at the bottom right corner is positivity in the tumor cells. CD3, red; Myc, green; 4',6-diamidino-2-phenylindole (DAPI), blue. (F) Comutation plots including the spectrum of somatic mutations and focal SCNAs. (G) Rearrangements of TCR genes identified through the MiXCR algorithm using WES data. The y-axis indicates each rearranged TCR gene with a certain complementarity-determining region 3 (CDR3) sequence. Distinct CDR3 regions are indicated by alternating colors within each sample; colors are indicated in descending order and do not indicate sequence identity.

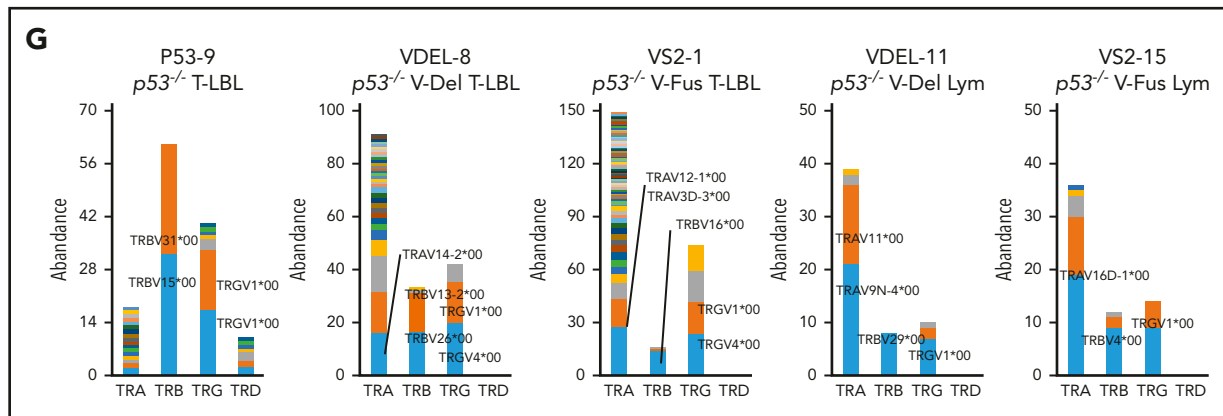


Figure 6. (Continued).

### Treatment with a bromodomain inhibitor prolongs overall survival of mice harboring VAV1-mutant tumors

We tested the *in vivo* effect of JQ1 using nude mice that had undergone secondary transplantation with T-LBL or Lym from *p53*<sup>-/-</sup> VAV1-*Tg* mice or T-LBL from *p53*<sup>-/-</sup> mice. Recipient mice were injected intraperitoneally with JQ1 at 3 mg/kg (*p53*<sup>-/-</sup> VAV1-*Tg* T-LBL, *n* = 7; Lym, *n* = 20; *p53*<sup>-/-</sup> T-LBL, *n* = 10) or with vehicle (*p53*<sup>-/-</sup> VAV1-*Tg* T-LBL, *n* = 10; Lym, *n* = 20; *p53*<sup>-/-</sup> T-LBL, *n* = 10) once every 2 days from day 7 after transplantation until animals died (Figure 7A). JQ1 prolonged overall survival (OS) of recipient mice transplanted with T-LBL or Lym from *p53*<sup>-/-</sup> VAV1 mice (Figure 7B-C). By contrast, OS of JQ1-treated recipient mice transplanted with T-LBL from *p53*<sup>-/-</sup> mice was comparable to that seen in vehicle-treated mice (Figure 7D).

### Discussion

Here, we report that expression of VAV1 mutants accelerates TCN development in the presence of *Trp53* deletion. Two kinds of VAV1 mutants, V-Fus and V-del, have similar oncogenic properties because tumors harboring either V-Fus or V-del mutant display similar phenotypes, GEPs, and genomic abnormalities. Although all TCNs seen in *p53*-null mice were immature T-LBL with CD24<sup>+</sup>TCR $\beta$ <sup>low</sup>, TCNs expressing VAV1 mutants exhibited more mature immunophenotypes, namely, T-LBL with CD24<sup>+</sup>TCR $\beta$ <sup>+</sup> and Lym.

PTCL-NOS in humans is classified as belonging to either PTCL-GATA3 or PTCL-Tbx21 subgroups, depending on molecular signature.<sup>29</sup> PTCL-GATA3 has a worse prognosis,<sup>29,30</sup> is characterized by high MYC expression,<sup>30</sup> and often shows complex genomic abnormalities with a high frequency of MYC amplifications.<sup>24</sup> Here, we report that Lym resembles human PTCL-GATA3: Lym tumors exhibit a Th2 phenotype based on tumor GEPs and cytokine profiles in sera of Lym-bearing mice. We also observed increased Myc expression and amplification of Myc locus in Lym tumors. Comparison of GEPs in mouse Lym and human PTCL-GATA3 further revealed features common to both (supplemental Figure 5G).

We observed Ccr4 expression as well as Gata3 expression on Lym tumor cells harboring VAV1 mutants, and others have reported that Ccr4 expression levels positively correlate with those of GATA3 in human PTCL-GATA3.<sup>31</sup> Mogamulizumab, a defucosylated anti-CCR4 antibody, is reportedly effective against some PTCLs that express CCR4 on tumor cells.<sup>32</sup> Therefore, PTCLs that harbor VAV1 mutations should be evaluated for CCR4 expression as mogamulizumab could be a treatment option.

Development of Lym with Th2 skewing and high Myc expression may be attributable to chronic active TCR signaling, considering that we observed VAV1 phosphorylation, a marker of active TCR signaling, in V-Fus-expressing nontumor T cells and Lym tumor cells (Figures 1D and 3Bii). TCR signaling reportedly activates cell-cycle-related activities, including Myc expression, and augments proliferation of mature T cells,<sup>33</sup> whereas sustained TCR signaling in T cells results in mature TCN development due to deregulation of proliferative signals.<sup>34</sup> In addition, it is known that tonic rather than acute TCR signaling instructs CD4 naive T cells to differentiate into Gata3-expressing Th2 rather than Th1 cells.<sup>35</sup> Indeed, we observed enrichment of cell-cycle-related gene sets (G2M checkpoint and E2F targets), and slightly elevated expression of Myc and Gata3, all of which occur downstream of TCR signaling,<sup>36,37</sup> in V-Fus-expressing CD4 T<sub>N</sub> and CD4 T<sub>mem</sub> prior to tumor development. Exacerbation of these activities represented by amplification of the Myc locus and the other oncogenic events occur as Lym develops.

In contrast, we did not observe VAV1 phosphorylation in V-Fus-expressing T-LBL tumor cells, suggesting that accelerated T-LBL development seen in mice harboring the V-Fus mutant is likely not due to TCR signal activation. V-Fus lacks the C-terminal SH3 domain, which is reportedly required for interaction with Notch1 intracellular domain (ICN1) and Cbl-b protein, a ubiquitin ligase that facilitates the degradation of ICN1 by Cbl-b.<sup>9</sup> Activation of Notch signaling due to overexpression of the ICN1<sup>38,39</sup> or gain of functions in the *NOTCH1* gene<sup>38,40</sup> reportedly lead to T-LBL development. Therefore, T-LBL development in mice harboring the V-Fus mutant may be attributable to Notch1 activation, although these mechanisms remain to be characterized. Enhanced Myc pathway activity seen in VAV1-mutant T-LBL may also be due to increased Notch1 signaling, as

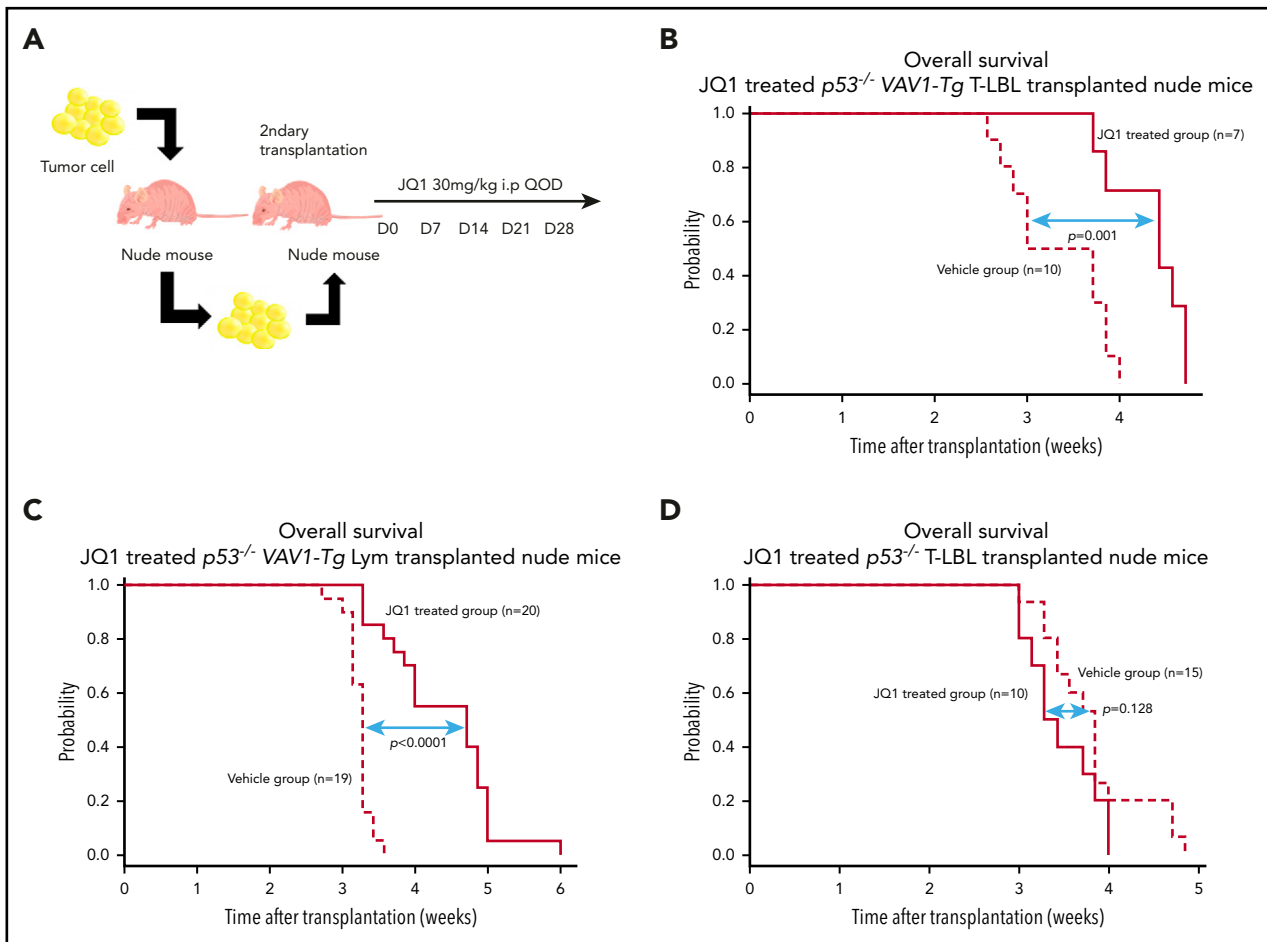


**Figure 7. Effects of bromodomain inhibitors on VAV1-mutant tumor cells.** (A) Schematic showing protocol used for vehicle or JQ1 treatment. Single-cell suspensions were prepared from spleens of nude mice transplanted with T-LBL or Lym from  $p53^{-/-}$  VAV1-Tg mice or T-LBL from  $p53^{-/-}$  mice and intraperitoneally injected into nude mice. JQ1 at 3 mg/kg was injected intraperitoneally into secondarily transplanted nude mice once every 2 days from day 7 until animals died. (B-D) Survival curves for vehicle- and JQ1-treated nude mice transplanted with T-LBL from  $p53^{-/-}$  VAV1-Tg mice (B), Lym from  $p53^{-/-}$  VAV1-Tg mice (C), or T-LBL from  $p53^{-/-}$  mice (D).

Myc transcription is reportedly directly regulated by Notch1 in T-LBL.<sup>41,42</sup>

In summary, we established mice expressing VAV1 mutants in T cells, enabling us to assess the oncogenic roles of these mutations in TCNs. Our mouse models may provide important tools in which to test new therapeutic strategies to antagonize these malignancies.

## Acknowledgments

The authors thank Elise Lamar for editorial assistance ([www.eliselamar.com](http://www.eliselamar.com)). The authors also thank Yutaka Suzuki, Kaoru Uchimar, and Makoto Yamagishi (University of Tokyo) for active discussion, and Yukari Sakashita and Hiroko Kunifuda for technical assistance. Mouse and cell illustrations (Figures 5I and 7A; supplemental Figure 3A) were supported by DBCLS TogoTV (<https://togotv.dbcls.jp/pics.html>).

This work was supported by Grants-in-Aid for Scientific Research (KAKENHI: 18K16077 [T.B.N.], 18H02834 [M.S.-Y.], 16H02660 [S.C.], and 19H03683 [S.C.]) from the Ministry of Education, Culture, Sports, and Science of Japan, and Japan Agency for Medical Research and Development (AMED) under grant numbers JP20ck0106544h and JPxxlm0203010 (M.S.-Y.) and JP16cm0106505h (S.C.).

## Authorship

Contribution: K.F. and M.S.-Y. performed experiments and analyzed data; M.F., T.S., Y. Suehara, T.B.N., S.S., S.Y., Y. Shiraishi, and K.C. collected data and were involved in this project; H.M., T.B.N., and K.O. stained samples and diagnosed; M.F., T.B.N., A.B., K.K., S.O., and J.I. provided GEP data for human AITL, PTCL-GATA3, ATL patient, and AITL mouse models; K.F., M.S.-Y., and S.C. generated the figures and tables and wrote this manuscript; M.S.-Y. and S.C. led the entire project; and all authors participated in discussions and interpretation of the data and results.

Conflict-of-interest disclosure: M.S.-Y. received funds from Celgene. K.K. received funds from Otsuka Pharmaceuticals, Takeda Pharmaceutical, and Chugai Pharmaceutical. K.O. received funds from Celgene and Daiichi Sankyo. S.C. received funds from Thyas, Takeda Pharmaceutical, Chugai Pharmaceutical, Kyowa-Kirin, Ono Pharmaceutical, Sanofi, and Astellas Pharmaceutical for research unrelated to this work. The remaining authors declare no competing financial interests.

ORCID profiles: K.F., 0000-0002-2729-5780; M.S.-Y., 0000-0001-7310-8045; H.M., 0000-0002-2356-3725; Y. Suehara, 0000-0001-7046-2196; S.S., 0000-0003-2491-3798; S.Y., 0000-0003-0886-0171; K.K., 0000-0002-8263-9902; S.O., 0000-0002-7778-5374; S.C., 0000-0001-7803-7338.

Correspondence: Shigeru Chiba, Department of Hematology, Faculty of Medicine, University of Tsukuba., 1-1-1 Tennodai, Tsukuba, Ibaraki

## Footnotes

Submitted 23 April 2020; accepted 16 September 2020; prepublished online on *Blood* First Edition 29 September 2020. DOI 10.1182/blood.2020006513.

The publication costs of this article were defrayed in part by page charge payment. Therefore, and solely to indicate this fact, this article is hereby marked "advertisement" in accordance with 18 USC section 1734.

## REFERENCES

1. Swerdlow SH, Campo E, Pileri SA, et al. The 2016 revision of the World Health Organization classification of lymphoid neoplasms. *Blood*. 2016;127(20):2375-2390.
2. Kataoka K, Nagata Y, Kitanaka A, et al. Integrated molecular analysis of adult T cell leukemia/lymphoma. *Nat Genet*. 2015;47(11):1304-1315.
3. Boddicker RL, Razidlo GL, Dasari S, et al. Integrated mate-pair and RNA sequencing identifies novel, targetable gene fusions in peripheral T-cell lymphoma. *Blood*. 2016;128(9):1234-1245.
4. Watatani Y, Sato Y, Miyoshi H, et al. Molecular heterogeneity in peripheral T-cell lymphoma, not otherwise specified revealed by comprehensive genetic profiling. *Leukemia*. 2019;33(12):2867-2883.
5. Abate F, da Silva-Almeida AC, Zairis S, et al. Activating mutations and translocations in the guanine exchange factor VAV1 in peripheral T-cell lymphomas. *Proc Natl Acad Sci USA*. 2017;114(4):764-769.
6. Boddicker RL, Razidlo GL, Feldman AL. Genetic alterations affecting GTPases and T-cell receptor signaling in peripheral T-cell lymphomas. *Small GTPases*. 2019;10(1):33-39.
7. Fujisawa M, Sakata-Yanagimoto M, Nishizawa S, et al. Activation of RHOA-VAV1 signaling in angioimmunoblastic T-cell lymphoma. *Leukemia*. 2018;32(3):694-702.
8. Van Vlierberghe P, Ferrando A. The molecular basis of T cell acute lymphoblastic leukemia. *J Clin Invest*. 2012;122(10):3398-3406.
9. Robles-Valero J, Lorenzo-Martin LF, Menacho-Marquez M, et al. A paradoxical tumor-suppressor role for the Rac1 exchange factor Vav1 in T cell acute lymphoblastic leukemia. *Cancer Cell*. 2017;32(5):608-623.e9.
10. Bustelo XR. Vav proteins, adaptors and cell signaling. *Oncogene*. 2001;20(44):6372-6381.
11. Han J, Das B, Wei W, et al. Lck regulates Vav activation of members of the Rho family of GTPases. *Mol Cell Biol*. 1997;17(3):1346-1353.
12. Michel F, Grimaud L, Tuosto L, Acuto O. Fyn and ZAP-70 are required for Vav phosphorylation in T cells stimulated by antigen-presenting cells. *J Biol Chem*. 1998;273(48):31932-31938.
13. Huang J, Tilly D, Altman A, Sugie K, Grey HM. T-cell receptor antagonists induce Vav phosphorylation by selective activation of Fyn kinase. *Proc Natl Acad Sci USA*. 2000;97(20):10923-10929.
14. Kuhne MR, Ku G, Weiss A. A guanine nucleotide exchange factor-independent function of Vav1 in transcriptional activation. *J Biol Chem*. 2000;275(3):2185-2190.
15. Costello PS, Walters AE, Mee PJ, et al. The Rho-family GTP exchange factor Vav is a critical transducer of T cell receptor signals to the calcium, ERK, and NF-kappaB pathways. *Proc Natl Acad Sci USA*. 1999;96(6):3035-3040.
16. Saveliev A, Vanes L, Ksionda O, et al. Function of the nucleotide exchange activity of vav1 in T cell development and activation. *Sci Signal*. 2009;2(101):ra83.
17. Fujikawa K, Miletic AV, Alt FW, et al. Vav1/2/3-null mice define an essential role for Vav family proteins in lymphocyte development and activation but a differential requirement in MAPK signaling in T and B cells. *J Exp Med*. 2003;198(10):1595-1608.
18. Zhang R, Alt FW, Davidson L, Orkin SH, Swat W. Defective signalling through the T- and B-cell antigen receptors in lymphoid cells lacking the vav proto-oncogene. *Nature*. 1995;374(6521):470-473.
19. Tarakhovskiy A, Turner M, Schaal S, et al. Defective antigen receptor-mediated proliferation of B and T cells in the absence of Vav. *Nature*. 1995;374(6521):467-470.
20. López-Lago M, Lee H, Cruz C, Movilla N, Bustelo XR. Tyrosine phosphorylation mediates both activation and downmodulation of the biological activity of Vav. *Mol Cell Biol*. 2000;20(5):1678-1691.
21. Yu B, Martins IR, Li P, et al. Structural and energetic mechanisms of cooperative auto-inhibition and activation of Vav1. *Cell*. 2010;140(2):246-256.
22. Eino D, Tsukada Y, Naito H, et al. LPA4-mediated vascular network formation increases the efficacy of anti-PD-1 therapy against brain tumors. *Cancer Res*. 2018;78(23):6607-6620.
23. Kanda Y. Investigation of the freely available easy-to-use software "EZ" for medical statistics. *Bone Marrow Transplant*. 2013;48(3):452-458.
24. Heavican TB, Bouska A, Yu J, et al. Genetic drivers of oncogenic pathways in molecular subgroups of peripheral T-cell lymphoma. *Blood*. 2019;133(15):1664-1676.
25. Zhou Y, Zhou B, Pache L, et al. Metascape provides a biologist-oriented resource for the analysis of systems-level datasets. *Nat Commun*. 2019;10(1):1523.
26. Subramanian A, Tamayo P, Mootha VK, et al. Gene set enrichment analysis: a knowledge-based approach for interpreting genome-wide expression profiles. *Proc Natl Acad Sci USA*. 2005;102(43):15545-15550.
27. Mootha VK, Lindgren CM, Eriksson KF, et al. PGC-1alpha-responsive genes involved in oxidative phosphorylation are coordinately downregulated in human diabetes. *Nat Genet*. 2003;34(3):267-273.
28. Nguyen TB, Sakata-Yanagimoto M, Fujisawa M, et al. Dasatinib is an effective treatment for angioimmunoblastic T-cell lymphoma. *Cancer Res*. 2020;80(9):1875-1884.
29. Iqbal J, Wright G, Wang C, et al; Lymphoma Leukemia Molecular Profiling Project and the International Peripheral T-cell Lymphoma Project. Gene expression signatures delineate biological and prognostic subgroups in peripheral T-cell lymphoma. *Blood*. 2014;123(19):2915-2923.
30. Manso R, Bellas C, Martin-Acosta P, et al. C-MYC is related to GATA3 expression and associated with poor prognosis in nodal peripheral T-cell lymphomas. *Haematologica*. 2016;101(8):e336-e338.
31. Amador C, Greiner TC, Heavican TB, et al. Reproducing the molecular subclassification of peripheral T-cell lymphoma-NOS by immunohistochemistry. *Blood*. 2019;134(24):2159-2170.
32. Ogura M, Ishida T, Hatake K, et al. Multicenter phase II study of mogamulizumab (KW-0761), a defucosylated anti-CC chemokine receptor 4 antibody, in patients with relapsed peripheral T-cell lymphoma and cutaneous T-cell lymphoma. *J Clin Oncol*. 2014;32(11):1157-1163.
33. Preston GC, Sinclair LV, Kaskar A, et al. Single cell tuning of Myc expression by antigen receptor signal strength and interleukin-2 in T lymphocytes. *EMBO J*. 2015;34(15):2008-2024.
34. Wang X, Werneck MB, Wilson BG, et al. TCR-dependent transformation of mature memory phenotype T cells in mice. *J Clin Invest*. 2011;121(10):3834-3845.
35. Miller AT, Wilcox HM, Lai Z, Berg LJ. Signaling through Itk promotes T helper 2 differentiation via negative regulation of T-bet. *Immunity*. 2004;21(1):67-80.
36. Zhu JW, Field SJ, Gore L, et al. E2F1 and E2F2 determine thresholds for antigen-induced T-cell proliferation and suppress tumorigenesis. *Mol Cell Biol*. 2001;21(24):8547-8564.
37. Guy CS, Vignali KM, Temirov J, et al. Distinct TCR signaling pathways drive proliferation and cytokine production in T cells. *Nat Immunol*. 2013;14(3):262-270.

38. Weng AP, Ferrando AA, Lee W, et al. Activating mutations of NOTCH1 in human T cell acute lymphoblastic leukemia. *Science*. 2004;306(5694):269-271.
39. O'Neil J, Grim J, Strack P, et al. FBW7 mutations in leukemic cells mediate NOTCH pathway activation and resistance to gamma-secretase inhibitors. *J Exp Med*. 2007;204(8):1813-1824.
40. Aster JC, Pear WS, Blacklow SC. Notch signaling in leukemia. *Annu Rev Pathol*. 2008;3:587-613.
41. Weng AP, Millholland JM, Yashiro-Ohtani Y, et al. c-Myc is an important direct target of Notch1 in T-cell acute lymphoblastic leukemia/lymphoma. *Genes Dev*. 2006;20(15):2096-2109.
42. Palomero T, Lim WK, Odom DT, et al. NOTCH1 directly regulates c-MYC and activates a feed-forward-loop transcriptional network promoting leukemic cell growth [published correction appears in *Proc Natl Acad Sci USA*. 2007;104(10):4240]. *Proc Natl Acad Sci USA*. 2006;103(48):18261-18266.